frontiers in Mechanical Engineering

ORIGINAL RESEARCH
published: 02 April 2019
doi: 10.3389/fmech.2019.00006

Atomistic Insights Into Lubricated Tungsten/Diamond Sliding Contacts

*Pedro A. Romero[1], Leonhard Mayrhofer[1], Pantcho Stoyanov[1,2], Rolf Merz[3], Michael Kopnarski[3], Martin Dienwiebel[1,2] and Michael Moseler[1,4,5]**

[1] Fraunhofer-Institute for Mechanics of Materials IWM–MicroTribology Center, Freiburg, Germany, [2] Karlsruhe Institute of Technology, Institute for Applied Materials, Karlsruhe, Germany, [3] Institut für Oberflächen- und Schichtanalytik (IFOS), University of Kaiserslautern, Kaiserslautern, Germany, [4] Physics Department, University of Freiburg, Freiburg, Germany, [5] Freiburg Materials Research Center, University of Freiburg, Freiburg, Germany

The reinforcement of coatings with diamond particles results in superior tribological performance in automotive applications. In addition to improving the coating's bulk properties, sliding of diamond on metallic counter bodies contributes to improved tribological performance. Therefore, in order to design better diamond-reinforced coatings, it is imperative to understand the atomistic mechanisms at sliding metal/diamond interfaces. Here, we investigate the interfacial tribochemical mechanisms leading to low friction in lubricated tungsten/diamond sliding contacts by combining reactive atomistic simulations with on-line tribometry experiments linked to chemical analysis. Reactive classical molecular dynamics simulations reveal the dehydrogenation of hexadecane lubricant molecules between tungsten/diamond contacts by proton transfer from the hexadecane to octahedral sites of the tungsten surface. Subsequent chemisorption of the radicalized hexadecane on dangling C-bond sites of the diamond surface leads to the formation of low-density hydrocarbon films, which significantly lower frictional resistance in the tribo-contact. Quasi-static density functional theory calculations confirm the classical molecular dynamics results and reveal that radicalized hydrocarbon molecules can also bond *via* C–O bonds on a WO_3 layer covering the tungsten counter surface. The on-line tribometry experiments confirm the reduction of friction under hexadecane lubrication, and *ex situ* chemical analysis by means of X-ray photoelectron spectroscopy (XPS), Auger electron spectroscopy (AES), and electron energy loss spectroscopy (EELS) provides evidence of the formation of a carbon-rich tribofilm on the diamond and tungsten-oxide surfaces as predicted by the atomistic simulations.

Keywords: molecular dynamics (MD), DFT, tribochemistry, hydrocarbon, diamond/tungsten, tribometry, XPS, AES

OPEN ACCESS

Edited by:
Roman Pohrt,
Technische Universität Berlin, Germany

Reviewed by:
Martin H. Müser,
Saarland University, Germany
Liran Ma,
Tsinghua University, China

***Correspondence:**
Michael Moseler
mos@iwm.fhg.de

Specialty section:
This article was submitted to Tribology, a section of the journal Frontiers in Mechanical Engineering

Received: *05 December 2018*
Accepted: *01 March 2019*
Published: *02 April 2019*

Citation:
Romero PA, Mayrhofer L, Stoyanov P, Merz R, Kopnarski M, Dienwiebel M and Moseler M (2019) Atomistic Insights Into Lubricated Tungsten/Diamond Sliding Contacts. Front. Mech. Eng. 5:6. doi: 10.3389/fmech.2019.00006

INTRODUCTION

Lubricated diamond/steel tribocouples exhibit amazingly small friction coefficients and wear under boundary lubrication conditions (Mehan and Hayden, 1981). Indeed, diamond particles are added to tribological coatings sliding against steel in order to reduce friction and improve wear resistance (Wang et al., 2005; Venkateswarlu et al., 2009; Kim et al., 2011; Yin et al., 2017). For instance, piston rings used in diesel engines showing superior tribological performance employ galvanic chromium

coatings that are filled with microscale diamond particles (Kennedy et al., 2014; Linsler et al., 2017). Therefore, since piston rings slide against metallic cylinder liners, the fundamental tribological mechanisms governing friction and wear in lubricated metal/diamond contacts are not only of academic (Mehan and Hayden, 1981) but also of industrial interest (Esser et al., 2004).

Although already used in technical applications, the mechanisms leading to ultralow friction in lubricated metal/diamond contacts are not well-understood. It is unclear whether diamond undergoes a crystalline/amorphous phase transition (Pastewka et al., 2011) or whether chemical mixing leads to the formation of carbides. Furthermore, the role of the lubricant is still elusive. It certainly plays an important role for friction reduction under boundary lubrication. Is it chemically inert and does it strongly physisorbs to the surface? Or is it susceptible to tribochemical reactions and chemisorbs on one of the tribopartners? These questions cannot be answered by macroscopic tribological experiments.

In this article, a hexadecane lubricated tungsten/diamond contact is studied as a simple model system for industrial metal/diamond combinations lubricated by complex engine oils. By combining atomic-scale simulations with on-line tribometry experiments, the interfacial chemical mechanisms leading to low friction between hexadecane-lubricated tungsten/diamond sliding contacts are elucidated. We perform classical molecular dynamics and *ab initio* density functional theory (DFT) molecular static simulations to understand the surface chemistry leading to the formation of carbon reaction layers that reduce friction in tungsten/diamond tribological contacts. The accompanying experiments employing an on-line tribometer as well as X-ray photoelectron spectroscopy (XPS), Auger electron spectroscopy (AES), and electron energy loss spectroscopy (EELS) *ex situ* analysis of the counter surfaces, corroborate these findings.

METHODS

Classical Molecular Dynamics Simulations

Reactive classical molecular dynamics (MD) simulations of tribologically sheared hexadecane ($C_{16}H_{34}$) lubricant molecules confined between a tungsten (100) and reconstructed diamond (100) surface are performed. Two different surface terminations of the diamond are considered. A reconstructed diamond (100) surface with complete surface H termination [dia(100)H] provides a lower limit of reactivity for an initially non-reactive diamond surface, while the unreconstructed diamond (100) without H passivation [dia(100)] provides an upper limit of reactivity—representing a fully reactive diamond surface as it occurs for instance after a wear event that removes passivation. The dimensions of the diamond substrate are $5.00 \times 2.50 \times 5.71$ nm^3, while the dimensions of the monocrystalline tungsten substrate are $5.06 \times 2.53 \times 5.70$ nm^3. For both counter bodies, contact occurs on their (100) surfaces while being sheared at 30 m/s under a contact pressure of 10 GPa. The tribocouple is thermostated at 300 K using a dissipative particle dynamics (DPD) thermostat (Groot and Warren, 1997) at the outer faces of the counter bodies with a dissipation constant of 5 eV ps nm^{-2} and a cutoff of 0.5 nm.

A 10-GPa pressure in the contact is established by applying the Pastewka–Moser–Moseler tribo-barostat (Pastewka et al., 2008). The simulations are performed using a screened version (Stoyanov et al., 2013a) of the bond-order potential for W-C-H material systems developed by Juslin et al. (2005) and applied by us for various tribological simulations of W-C-H systems (Stoyanov et al., 2013a,b, 2014, 2015).

Density Functional Theory Quasi-Static Calculations

In order to verify the surface chemistry observed in the classical molecular dynamics simulations and to extend the numerical investigations to oxide surfaces, electronic structure calculations are performed employing the DFT (Hohenberg and Kohn, 1964; Kohn and Sham, 1965) as implemented in the VASP software suite (Kresse and Hafner, 1993, 1994) along with projector augmented-wave (PAW) potentials (Blöchl, 1994; Kresse and Joubert, 1999) for the simulated elements (i.e., W, C, O, H) and the PBE (Perdew et al., 1996) generalized gradient approximation to the XC potential. Structural relaxations are performed until the convergence criterion of a maximal force of 0.2 eV/nm acting on a single atom is reached. The Kohn–Sham wave functions are expanded in a plane wave basis using an energy cutoff of 400 eV. Periodic boundary conditions are applied along all directions. Chemical reaction energies are calculated as $\Delta E = E_{Rct} - E_{Prod}$, where E_{Rct} and E_{Prod} are the DFT ground state energies of the reactant and product states, respectively. With this definition, positive reaction energies indicate exothermic processes.

First, in order to verify the stability of hydrocarbon molecules in tungsten/diamond contacts, butane (C_4H_{10}) molecules confined between tungsten (100), reconstructed H-passivated diamond (100), and WO_3 (001) surfaces are relaxed quasi-statically under increasing normal pressures up to ∼70 GPa. For these simulations, in order to successively increase the normal pressure, the simulation box is reduced step by step along the surface normal, and the system is quasi-statically relaxed at each step. Additionally, radicalized butane (i.e., C_4H_9) molecules are relaxed on fully and partially passivated (100) diamond surfaces in order to study the removal of H passivation from the diamond surface by hydrocarbon radicals. Furthermore, the chemical adsorption energies of hydrocarbon molecules and radicals on diamond, tungsten, and tungsten oxide surfaces with reactive sites are determined.

Tribometry Experiments and Characterization

Friction and wear measurements are conducted using an "on-line" tribometer, equipped with a force sensor, a holographic microscope, and an atomic force microscope, permitting the monitoring of topographical changes after each cycle. The instrument is described in detail elsewhere (Korres and Dienwiebel, 2010). The experiments are performed on a 99.9 wt.% tungsten plate in the "as-rolled" condition and polished down to an rms roughness of 34 ± 4 nm with no significant

influence on the near surface structure or the chemical composition (as verified by SEM and XPS analyses). A diamond sphere with a radius of 1.5 mm and a roughness of 1.2 nm was used as the counter surface. The experiments are performed with a sliding velocity of 5 mm/s and an initial normal load of 2 N in reciprocating slide mode. The worn surfaces (i.e., plates, tips, and wear material) are characterized by *ex situ* chemical and structural analyses using XPS, AES, and EELS. Lateral elemental concentration distributions are also obtained by parallel imaging XPS.

RESULTS AND DISCUSSION

Reactive Classical Molecular Dynamics Study of Hydrocarbon-Lubricated Tungsten/Diamond Systems

We used reactive classical molecular dynamics to investigate hexadecane-lubricated tungsten/diamond tribocouples. Since the typically experiments are performed under ambient conditions, contact is expected to mainly occur between passivated diamond surfaces and tungsten oxide counter surfaces. Unfortunately, current classical MD simulations are restricted to systems containing W-C-H (Juslin et al., 2005), since an accurate force field for W-C-O-H is not available yet. Therefore, in this section, simulations of hexadecane-lubricated tungsten/diamond tribopairs are presented with the intention of providing atomistic insights into the generic chemistry between hydrocarbon molecules in a sliding metal/diamond contact. In the next section, these results will be verified and extended to W-C-O-H systems using DFT simulations.

Figure 1 presents the results of our classical reactive MD simulations. Snapshots of the hydrocarbon-lubricated simulations with a bare W(100) surface and an H-terminated reconstructed diamond (100) surface are shown in **Figure 1A** at time instances during the initial pressurization phase ($t = 0.04$ ns), the subsequent shearing phase ($t = 4.5$ ns), and after the final separation ($t > 4.7$ ns) of the counter surfaces. The same instances for the case without H termination of the reconstructed diamond surface are shown in **Figure 1B**. Interestingly, in both cases—W(100)/$C_{16}H_{34}$/dia(100)H and W(100)/$C_{16}H_{34}$/dia(100)—a thin hydrocarbon film has formed on the diamond surface (see **Figures 1A,B** for $t > 4.7$ ns). We note that this film has a lower density for W(100)/$C_{16}H_{34}$/dia(100)H and that in this case, also the tungsten surface carries a chemisorbed hydrocarbon fragment.

The chemical reactions leading to the formation of these films can be described as follows. Upon pressurization and shearing of hydrocarbon molecules (such as $C_{16}H_{34}$) between a bare W(100) surface and a fully passivated diamond (100) surface, hydrogen atoms dissociate from the $C_{16}H_{34}$ chains and diffuse mainly into the uppermost layers of the tungsten [see the second snapshot at ($t = 4.5$ ns) in **Figures 1A,B**]. The sliding motion then occurs between the H-enriched uppermost W layers and the degraded hydrocarbon molecules. As shearing under high pressure continues, radical sites on the hydrocarbon chains are pushed against the diamond surfaces and react with surface hydrogen atoms. This leads to partial dehydrogenation of the H-passivated diamond counter surface and results in the creation of dangling C bonds on the diamond. Eventually, radicalized hydrocarbon molecules bind to the diamond surface on these dangling C bonds *via* C–C covalent bonds. This can be clearly seen in **Figures 1C,D**, where the hydrocarbon molecules remain attached to the diamond surface after retraction of the counter surfaces. **Figure 1F** presents a close-up view of **Figure 1A**, highlighting the first H atoms that are dissociated from the $C_{16}H_{34}$ molecules and adsorbed on octahedral sites of the bcc tungsten surface. The first anchoring of a radicalized hydrocarbon on the partially dehydrogenated diamond (100) surface is displayed in **Figure 1G**. Interestingly, a large amount of lubricant H atoms has entered the tungsten lattice before the first hydrocarbon anchoring occurred. This indicates that many hydrocarbon molecules have already been radicalized before the anchoring reactions start.

The accumulation of hydrogen atoms within the tungsten lattice is a very clear sign that the original $C_{16}H_{34}$ molecules are significantly degraded under high-pressure shearing between bare tungsten and fully passivated diamond surfaces. Upon retraction of the sliding counterbodies, as shown in **Figure 1C**, the hexadecane chains remain bonded to the diamond surface, and most of the hydrogen atoms are located within the tungsten specimen. As expected, this phenomenon is more evident in the case of a non-hydrogen-terminated (and thus more reactive) diamond surface sliding against tungsten, where a higher number of dangling C bonds on the radicalized $C_{16}H_{34}$ chains can bond to dangling C bonds on the diamond surface (compare close-up image of the sliding interface in **Figure 1C** with that in **Figure 1D** where the diamond surface was not H terminated). These simulations show that during hydrocarbon-lubricated sliding between diamond and tungsten, the carbon-rich layer stemming from the lubricant attaches preferentially to the diamond counter surface with only very minor bonding onto the H-enriched tungsten surface.

The evolution of the shear stress τ and friction coefficient μ of the tungsten/diamond contacts is displayed in **Figure 1E**. For both the W(100)/$C_{16}H_{34}$/dia(100) and the W(100)/$C_{16}H_{34}$/dia(100)H sliding systems, the local friction coefficient $\mu = \frac{\tau}{p}$ exhibits an ultralow value of $\mu \approx 0.05$. Interestingly, in our classical MD simulations, the tungsten surface does not form any mixed WC phase in the presence of a hydrocarbon lubricant. If this were to happen, the hydrocarbon lubricant molecules would be consumed by the W surface and cold welding would lead to much higher friction coefficients.

Before we turn to the experimental investigation of a hexadecane-lubricated tungsten/diamond contact, a critical assessment of our classical simulations is in order. Since these experiments are performed under ambient conditions, oxygen atoms from atmospheric O_2 and H_2O are expected to play an important role. Unfortunately, we are currently not able to reliably model oxygen with classical reactive molecular dynamics, and therefore, more advanced simulation tools are needed to elucidate the degree of hydrocarbon radicalization and bonding between hydrocarbon radicals and reactive sites on tungsten oxide surfaces.

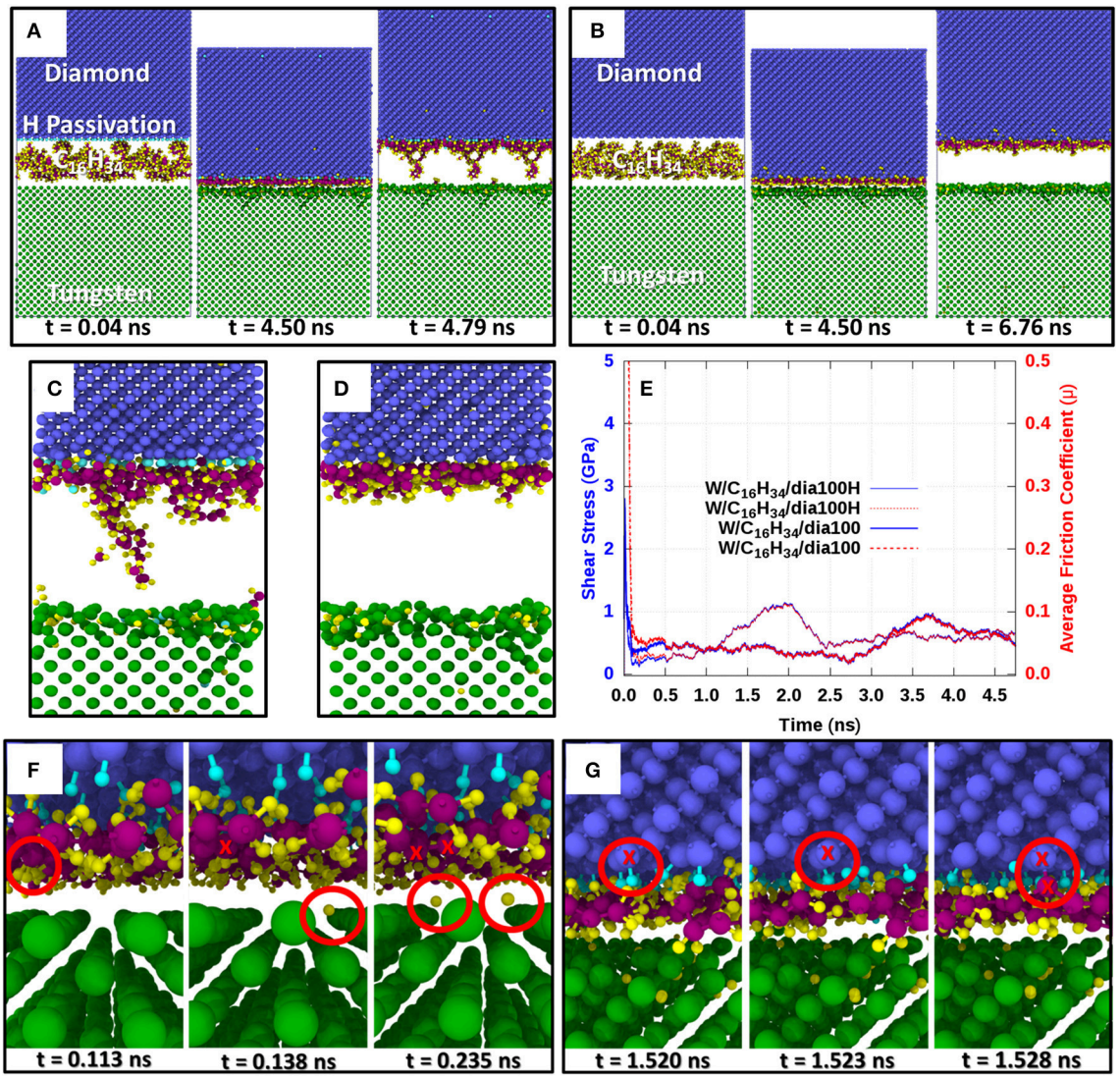

FIGURE 1 | Classical molecular dynamics simulations of hexadecane-lubricated tungsten/diamond tribocouples. Diamond carbon atoms are colored in blue, W atoms in green, H atoms in yellow, hexadecane C atoms in purple, and H atoms terminating the diamond surface in cyan. The lower surface is always a bare tungsten (100) surface. **(A)** Evolution of the lubricated tribocouple with H termination of the reconstructed diamond (100) surface W(100)/$C_{16}H_{34}$/dia(100)H. **(B)** Evolution of the lubricated tribocouple without H termination of the reconstructed diamond (100) surface W(100)/$C_{16}H_{34}$/dia(100). **(C,D)** Close-up views of the contact interface after retraction for the cases in **(A)** and **(B)**, respectively. The plot in **(E)** shows the evolution of shear stress (solid blue lines) and coefficient of friction (dotted red lines) for W(100)/$C_{16}H_{34}$/dia(100)H and W(100)/$C_{16}H_{34}$/dia(100). Close-up views of the initial chemical reactions observed for W(100)/$C_{16}H_{34}$/dia(100)H are depicted in **(F)** and **(G)**. **(F)** Initial radicalization of $C_{16}H_{34}$ hydrocarbons after dissociation of H atoms while in sliding contact under high pressure (~10 GPa). **(G)** First bonding of radicalized hydrocarbons on the diamond surface after the dehydrogenation of the initially fully H-passivated diamond (100) surface.

Density Functional Theory Investigations of the Reactivity of Lubricated W and Diamond Surfaces

DFT electronic structure calculations were performed to verify the hydrocarbon radicalization, hydrogen diffusion, and subsequent bonding of hydrocarbon radicals to the diamond observed in our classical MD simulations. Of course, DFT MD sliding simulations with system sizes and simulation times similar to those in the classical MD simulations are impossible with current computer resources. However, we can perform quasi-static pressure relaxation DFT simulations with chemically similar but smaller hydrocarbon molecules confined between diamond and W surfaces at different normal pressures. Under these conditions, the radicalization of hydrocarbons under high pressure and the subsequent bonding of the radicalized molecules on the counter surfaces can be studied. It is already expected that compressing hydrocarbon molecules between non-passivated diamond surfaces will result in a high reactivity between the molecules and the surface, which would include generation of radicals and bonding of these

radicals on the dangling bonds of the diamond surface. This uninteresting case was not simulated here. Instead, the lower limit of surface reactivity was considered by studying hydrogen-passivated diamond (100) surface as well as a bare tungsten (100) surface.

First, **Figure 2A** shows the DFT relaxation of butane molecules (C_4H_{10}) between reconstructed and fully H-passivated diamond (100) surfaces. In this case, it is impossible to generate hydrocarbon radicals by increasing the contact pressure up to ∼69 GPa, where the simulations are stopped. Conversely, as shown in **Figure 2B**, successively compressing butane between bare W(100) surfaces results in the generation of hydrocarbon radicals and in the adsorption of the dissociated H atoms on the tungsten surfaces for pressures below 10 GPa. We note that the radical formation is observed in the DFT simulations without thermal activation, such that the critical pressure for radical formation obtained in the quasi-static calculations is an upper limit for the critical pressure at finite temperature. Recall that the classical MD simulations presented in **Figure 1** show that once H atoms are dissociated from the hydrocarbon chains, the majority of these freed H atoms preferentially occupy interstitial sites close to the tungsten surface. Hence, a bare tungsten surface is able to radicalize hydrocarbon molecules and absorb and retain dissociated H atoms within its lattice. This verifies the hydrocarbon radicalization and H absorption predicted by the classical MD simulations in **Figure 1**.

In addition, the classical simulations in **Figure 1** predict that once hydrogen atoms are dissociated from the lubricant, the radicalized hydrocarbon molecules bond onto dangling C bonds of the diamond surface. These predictions are also verified by the formation energies presented in **Figures 2C–F**. Even in the extreme case of a fully reconstructed and H-passivated (100) diamond surface, the radicalized molecules can remove H atoms from the diamond surface as indicated by the 0.11-eV formation energy shown in **Figure 2C**. Here, a positive formation energy indicates an exothermic reaction. If there are dangling C bonds on the diamond (100) surface, the radicalized hydrocarbons can bond to the diamond surface through C–C covalent bonds with significant gains in energy. As shown in **Figure 2D**, if the hydrocarbon molecule is radicalized due to an H atom vacancy at the end of the molecule, there is an exothermic energy gain of 4.16 eV, while as shown in **Figure 2E**, if the radical site is in the middle of the hydrocarbon molecule, the exothermic energy gain is slightly reduced to 3.33 eV. Both of these energy values are significantly higher than the highest exothermic energy gain of 1.44 eV obtained by bonding a radical hydrocarbon (with an H missing at the tail of the molecule) on a hydrogen-saturated W(100) surface, as shown in **Figure 2E**. Even in the case of a W surface without any adsorbed H, the exothermic formation energy gain of 2.64 eV is still significantly lower than that of the diamond surface. These energy values indicate that radical hydrocarbons are preferentially bonded onto the diamond surface when the other counter surface is a bare W surface as in the classical MD simulations presented in **Figure 1**.

Density Functional Theory Investigations of the Reactivity of Lubricated WO_3

In experiments under ambient conditions, most of the tungsten surface is covered by tungsten oxide (WO_3), which means that hydrocarbon molecules would be compressed between a WO_3 and a diamond surface. This situation could not be modeled with classical MD; however, it can be investigated quasi-statically with DFT. If hydrocarbon molecules are compressed between (100) WO_3 surfaces with an oxygen-deficient pure W termination or a stoichiometric ½ ML coverage with additional oxygen ions, no hydrocarbon radicalization was observed with pressures up to 12 GPa (i.e., the yield stress of pure crystalline WO_3), where plastic deformation starts to occur within WO_3 (not shown here). However, as displayed in **Figure 3A**, as soon as an oxygen coverage beyond ½ ML is simulated, hydrocarbon radicalization evolves quickly at relatively low pressures of approximately 1.5 GPa (metallic W required 10 GPa before hydrocarbon radicalization). Therefore, on the tungsten/tungsten oxide side of the tribocouple, the most likely sources of hydrocarbon radicalization are the highest tungsten oxide asperities, followed by exposed patches of pure tungsten (presumably generated by wear events). Hydrocarbon radicalization on the diamond side of the tribocouple could also occur at exposed patches of non-passivated diamond at asperity peaks. However, since diamond is the harder material in the tribocouple and if the system is in a humid environment, the diamond surface is expected to remain mostly passivated with only a few sites with dangling C bonds where hydrocarbon radicals or free H atoms could quickly bond. Therefore, we expect the tungsten/tungsten oxide side of the tribocouple to be the main driver of hydrocarbon radicalization.

It is also important to look into the ability of WO_3 surfaces to adsorb hydrocarbon radicals. **Figures 3B–D** shows the energies for the adsorption of a C_4H_9 radical (with an H missing on a tail) on an oxygen-deficient, a stoichiometric oxygen-saturated, and a fully oxygen-saturated WO_3 (100) surface with exothermic energy gains of 1.32, 2.02, and 1.82 eV, respectively. Comparing these formation energies with those in **Figure 2**, it can be concluded that in a hydrocarbon-lubricated tungsten/diamond contact, radicalized hydrocarbon molecules are more strongly adsorbed on dangling carbon bonds of the diamond surface, but these radicals can also react with the tungsten side by bonding directly to the tungsten oxide surface. In case of a stoichiometrically O-terminated WO_3 (100) surface, the radicalization and subsequent adsorption of a butane molecule *via* a C–O bond is slightly exothermic with a reaction energy of 0.27 eV (see **Figure 3E**). Interestingly, as shown in **Figure 3F**, the radicalization and bonding of the radical *via* a C–OH group on a WO_3 surface with slightly overstoichiometric O coverage (i.e., ½ ML + 1 O-ion coverage; see **Figure 3F**) result in a significant exothermic energy gain of 4.40 eV. However, as shown in **Figure 3G**, this molecule can be easily desorbed as a C_4H_9OH molecule with a modest energy cost of 0.67 eV. Hence, the presence of tungsten oxide surfaces can lead to the addition of oxygen-containing functional groups to the hydrocarbon lubricant molecules, which after a subsequent radicalization could be transferred to the diamond surface. This

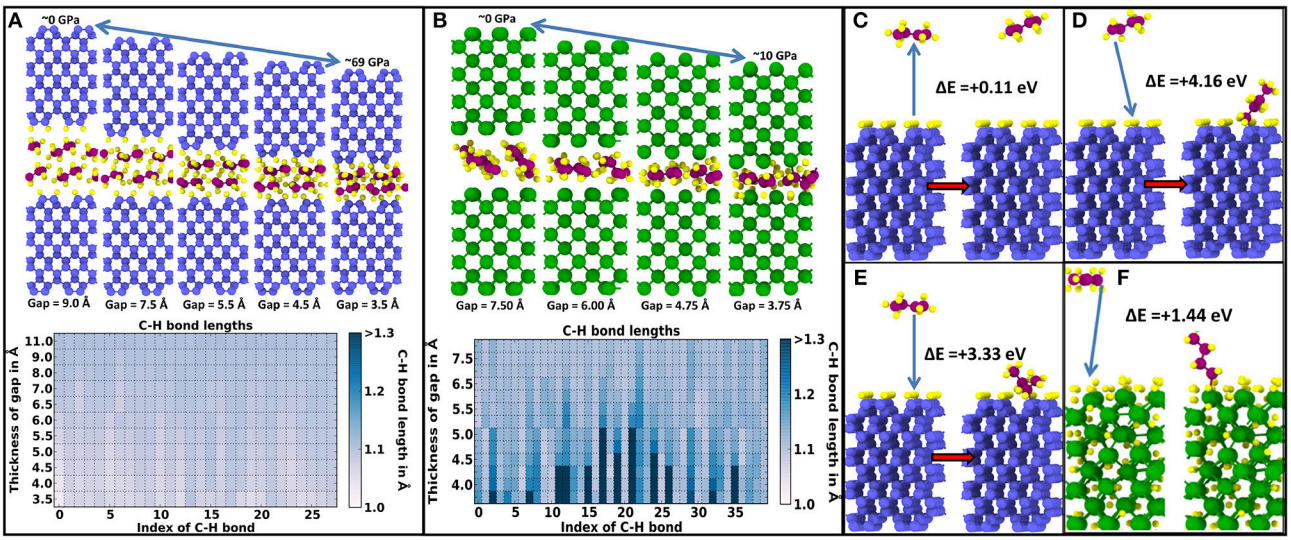

FIGURE 2 | Density functional theory (DFT) quasi-static pressure relaxation simulations showing the activation and sometimes radicalization of butane (C_4H_{10}) molecules confined between diamond (100) and W (100) surfaces. Coloring of atoms is as follows: diamond C atoms are blue, H atoms yellow, butane C atoms purple, and W atoms green. **(A)** Stability of hydrocarbon C_4H_{10} molecules indicated by an almost constant C–H bond length between molecules confined between reconstructed H-passivated (100) diamond surfaces. **(B)** Progressive elongation and eventual breaking of some C–H bonds in the C_4H_{10} molecules with decreasing gap separation between bare W(100) surfaces. In **(A)** and **(B)**, the top panel shows selected snapshots with decreasing interface gap (i.e., increasing pressure), while the bottom panel shows the elongation of each C–H bond with decreasing interface gap. **(C)** Energy gain during proton transfer from a diamond (100) surface to a C_4H_9 radical. **(D)** Adsorption of a $CH_2C_3H_7$ radical (with an H missing on a tail group) on a diamond (100) surface with one dangling C bond. **(E)** Adsorption of a CH_3-CH–C_2H_5 radical (with one H missing on an inner C group) on a diamond (100) surface with one dangling C bond. **(F)** Adsorption of a $CH_2C_3H_7$ radical (with an H missing on a tail group) on a hydrogen-saturated tungsten (100) surface.

would result in a hydrocarbon film on the diamond tribopartner that contains oxygen.

Friction and Wear Experiments

Tribological experiments with hexadecane-lubricated tungsten/diamond interfaces were conducted to compare with the atomistic simulations presented above. The evolution of the friction coefficient and wear rate during hexadecane-lubricated sliding of diamond against tungsten is presented in **Figure 4A**. In the experiments, the coefficient of friction remains relatively low and constant with an average value of $\mu \sim 0.05$ despite the fact—as we know from earlier studies—that the experiments are conducted in the mixed or boundary lubrication regime (Stoyanov et al., 2013b). Interestingly, nearly no running-in phase was observed, which could be attributed to the low initial roughness and/or the filling-in of the contact interface by lubricant molecules. This hydrocarbon-induced reduction in friction is typical for lubricated metal/diamond contacts (Mehan and Hayden, 1981). The initial wear rate of ~23 nm/m as measured through topography maps quickly decreased to a value of <0.7 nm/m at the 1,000th cycle. Inset images of the wear track after 50 and 1,000 cycles are shown in **Figure 4A**.

XPS *ex situ* analysis of the worn diamond surface after the test in **Figure 4A** is presented in **Figure 4B**. The XPS depth profile in **Figure 4B** indicates predominately carbon with some small traces of oxygen. The SEM inset image of the diamond tip displayed in **Figure 4B** clearly indicates a certain degree of material transfer. To further investigate this material transfer, EELS analysis is performed on the transferred material on the worn diamond tip. **Figure 4C** presents the cross section of a particle as well as EELS elemental mapping that indicates a high carbon content, some traces of oxygen, and a small amount of tungsten. The transfer of oxygen and tungsten provides evidence that there is material transfer from the tungsten surface to the diamond tip. The high carbon content observed as transfer material on the diamond tip most likely originates from the hydrocarbon molecules that degrade and bond to the diamond tip. However, the possibility of formation of an amorphous carbon layer emerging from the diamond itself cannot be excluded by *ex situ* XPS and EELS analysis of the diamond tip alone. Nevertheless, as indicated by the atomistic simulations above, the hydrocarbon molecules can be easily degraded when in contact with bare tungsten and tungsten oxide surfaces under high pressure, and these radicalized molecules can then bond most favorably on reactive sites on the diamond surface. The apparent pressure in the experiments was on the order of MPas. However, the local pressures at asperity level are expected to be on the order of GPas. A g_{rms} of 0.004 was measured for the polished tungsten plate, which, based on Persson's theory (Persson, 2006), predicts an average pressure of 1 GPa at the asperity level. Keeping in mind that there is a distribution of asperity pressure around an average value of 1 GPa, we also expect pressure at the asperity level well above 1 GPa (i.e., up to 10 GPa).

Next, we report the chemical analysis of the tungsten surface. **Figure 5A** presents an SEM image of the wear track on the tungsten plate after hexadecane-lubricated sliding against

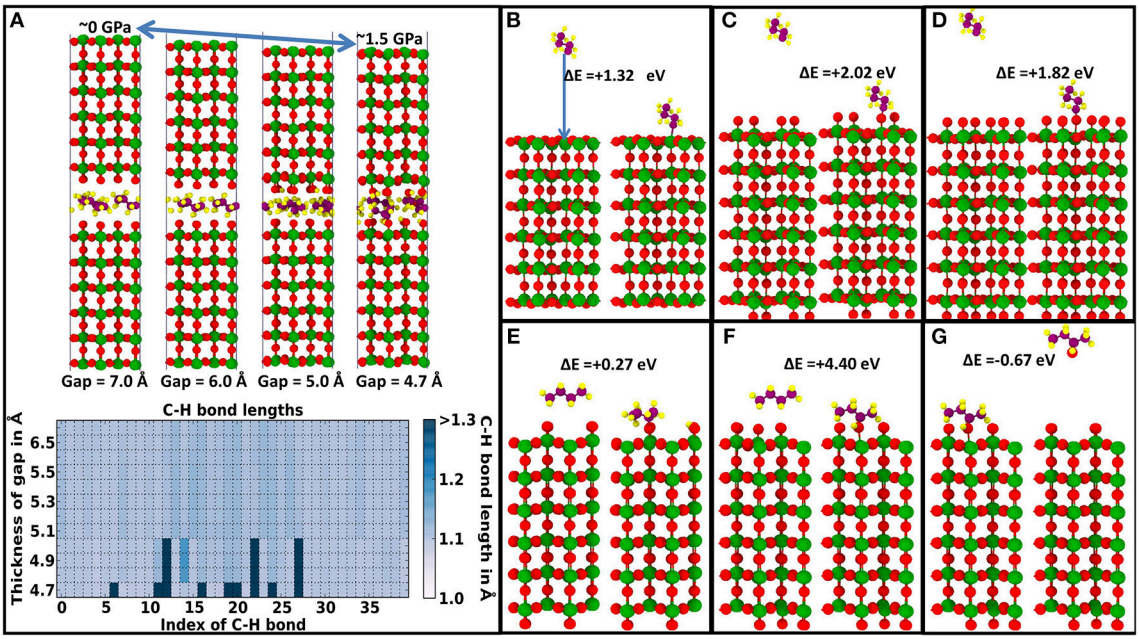

FIGURE 3 | Radicalization and adsorption of hydrocarbon molecules on WO_3 surfaces. Coloring of atoms is as follows: W atoms are green, O atoms red, H atoms yellow, and hydrocarbon C purple. **(A)** DFT quasi-static pressure relaxation showing the sudden elongation and breaking of some C–H bonds in butane (C_4H_{10}) molecules with increasing pressure between reactive WO_3 surfaces. In **(A)**, the top panel shows selected snapshots with decreasing interface gap (i.e., increasing pressure), while the bottom panel depicts the elongation of each C–H bond with decreasing interface gap. Adsorption of a CH_2-C_3H_7 radical (an H missing at the tail) on **(B)** an oxygen-deficient purely W-terminated WO_3 (100) surface, **(C)** a stoichiometrically (i.e., ½ ML O-ion coverage) oxygen-saturated WO_3 (100) surface, and **(D)** a fully oxygen-saturated WO_3 (100) surface. Generation of a $C_2H_5CHCH_3$ radical (a missing H atom in the interior) and its adsorption after dissociation of an H atom from a C_4H_{10} molecule on **(E)** a stoichiometrically O-terminated (i.e., ½ ML O-ion coverage) WO_3 (100) surface and **(F)** a WO_3 (100) surface with one more O-ion than stoichiometrically necessary (i.e., ½ ML + 1 O-ion coverage). **(G)** Desorption energy of a C_4H_9OH molecule from a WO_3 surface with ½ML + 1 O oxygen [after the adsorption event shown in **(F)**].

diamond. The AES analysis maps in **Figure 5B** clearly show an increase in the oxide content on the worn surface compared to the unworn surface, which is typical for metallic sliding contacts and has been reported numerous times (Rigney, 2000; Fu et al., 2003; Scherge et al., 2003; Stoyanov et al., 2013a). Interestingly, the carbon content is noticeably higher in the worn regions compared to the unworn ones. To provide a better understanding of this carbon-based layer (i.e., increased carbon concentration) in the case of the lubricant, we looked at the bonding behavior of the carbon on the tungsten surface using XPS detail analysis as shown in **Figure 5C**. The analysis suggests that all carbon atoms, not bound inside aliphatic hydrocarbon chains, are predominantly bonded to oxygen without any evidence of carbon bonding with tungsten *via* C–W bonds as in tungsten carbide. Conversely, the oxygen is also bonded with tungsten in the form of WO_3 on the surface of the tungsten specimen. It is likely that the increased oxide content on the worn surface promotes the formation of the carbon-based layer on the worn surface. The carbon-based layer found on the W surface after lubricated sliding most likely stems from the hydrocarbon molecules rather than the diamond tip as suggested by our DFT simulations.

The DFT simulations verified the formation of a hydrocarbon film on the diamond counter surface and additionally showed that hydrocarbon molecules can radicalize and chemisorb *via* C–O bonds on WO_3 surfaces, suggesting that the lubricant-derived hydrocarbon films also form on tungsten counter surfaces with WO_3 passivation. These processes are summarized in graphical form in **Figure 6** by presenting one possible reaction path starting from a worn W/WO_3 surface, a passivated diamond surface, and pristine hydrocarbon lubricant molecules between the tungsten/diamond interface (**Figure 6A**). Next, as sketched in **Figure 6B**, the hydrocarbon molecules are radicalized as they are sheared under high pressures against patches of WO_3 and W on the worn tungsten surface. Once several hydrocarbon molecules have been radicalized and as shearing under high pressure continues (**Figure 6C**), these hydrocarbon radicals can remove some of the H atoms or OH groups from the passivated diamond surface. Subsequently, the other radicals can covalently bond to the diamond surface at sites with dangling C bonds (**Figure 6D**).

Finally, we note that we could not perform the DFT simulations with hexadecane $C_{16}H_{34}$ molecules because DFT simulations are computationally very expensive and typically limited to a few 100 atoms. However, we also note that even though the DFT simulations were performed with short hydrocarbon molecules (i.e., butane C_4H_{10}), we expect a very similar reaction process for longer hydrocarbon molecules (i.e.,

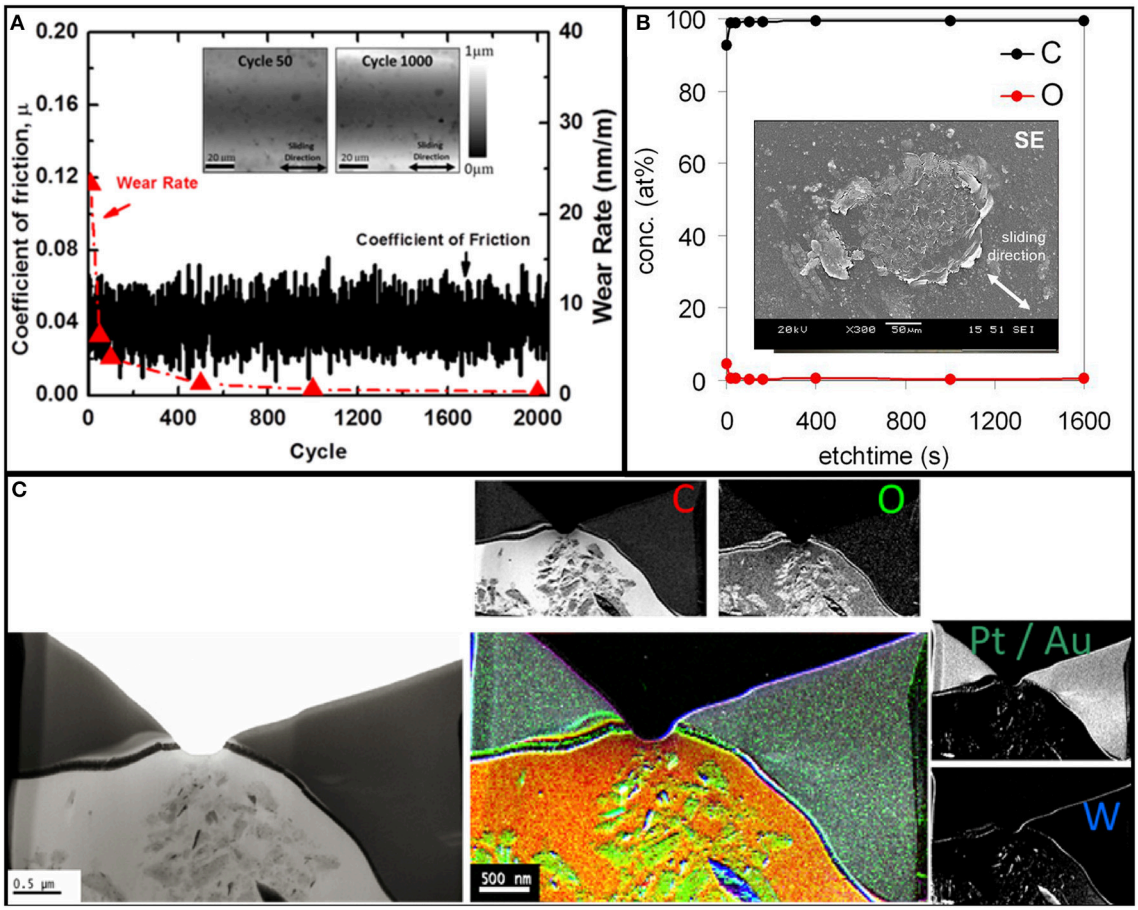

FIGURE 4 | (A) Coefficient of friction and wear rate vs. cycle for diamond sliding against tungsten under hexadecane-lubricated conditions. The inserts show images of the wear track after 50 and 1,000 cycles obtained using the on-line tribometer. Chemical analysis of the worn diamond surface with **(B)** showing an X-ray photoelectron spectroscopy (XPS) depth profile of the worn diamond surface with an SEM inset of the diamond surface after sliding. **(C)** Electron energy loss spectroscopy (EELS) analysis of a wear material particle on the diamond counter surface generated during sliding.

hexadecane $C_{16}H_{34}$). To provide some evidence for this, we calculated the radical formation energy for both C_4H_{10} and $C_{16}H_{34}$ molecules. An endothermic radical formation energy value of 2.07 eV was obtained for both C_4H_{10} and $C_{16}H_{34}$ for dehydrogenation in the middle of the molecular chain. For dehydrogenation at the tail end of the molecular chain, endothermic radical formation energy values of 2.26 and 2.25 eV were obtained for C_4H_{10} and $C_{16}H_{34}$, respectively. This is a good indication that C_4H_{10} and $C_{16}H_{34}$ will undergo a very similar radicalization process when sheared under high pressure between diamond/W/WO_3 sliding interfaces. Additionally, in a different study (Kuwahara et al., 2019), short $C_7H_{12}O_2$ and long $C_{18}H_{34}O_2$ acid molecules, which have different molecular lengths but the same reactive centers, were investigated using tight binding, which is computationally less expensive than DFT. In that study, it was shown that short cis-heptanoic acid ($C_7H_{12}O_2$) molecules undergo very similar tribochemical reactions as the longer oleic acid ($C_{18}H_{34}O_2$) molecules during shearing under high pressure between sliding ta-C counter surfaces. Therefore, we expect C_4H_{10} and $C_{16}H_{34}$ confined between diamond/W/WO_3 surfaces to follow very similar reaction paths with only minor differences in the pressure and energy required for the reactions.

CONCLUSION

Lubricated metal/diamond contacts exhibit noticeably low friction (Mehan and Hayden, 1981); however, the atomistic mechanisms for this phenomenon are still unclear. Here, we investigated the interfacial tribochemical mechanisms leading to low friction in lubricated tungsten/diamond sliding contacts using reactive atomistic simulations and an on-line tribometer linked to chemical analysis. First, reactive classical molecular dynamics simulations of tungsten (100) sliding against diamond (100) under high pressure revealed the radicalization of hydrocarbon molecules by proton transfer to the tungsten surface and their subsequent chemisorption onto dangling C bonds on the diamond surface. This results in the formation of hydrocarbon films that chemisorb on the diamond surface. Despite the small number of lubricant molecules between the tungsten and the diamond surface, an ultralow friction of μ =

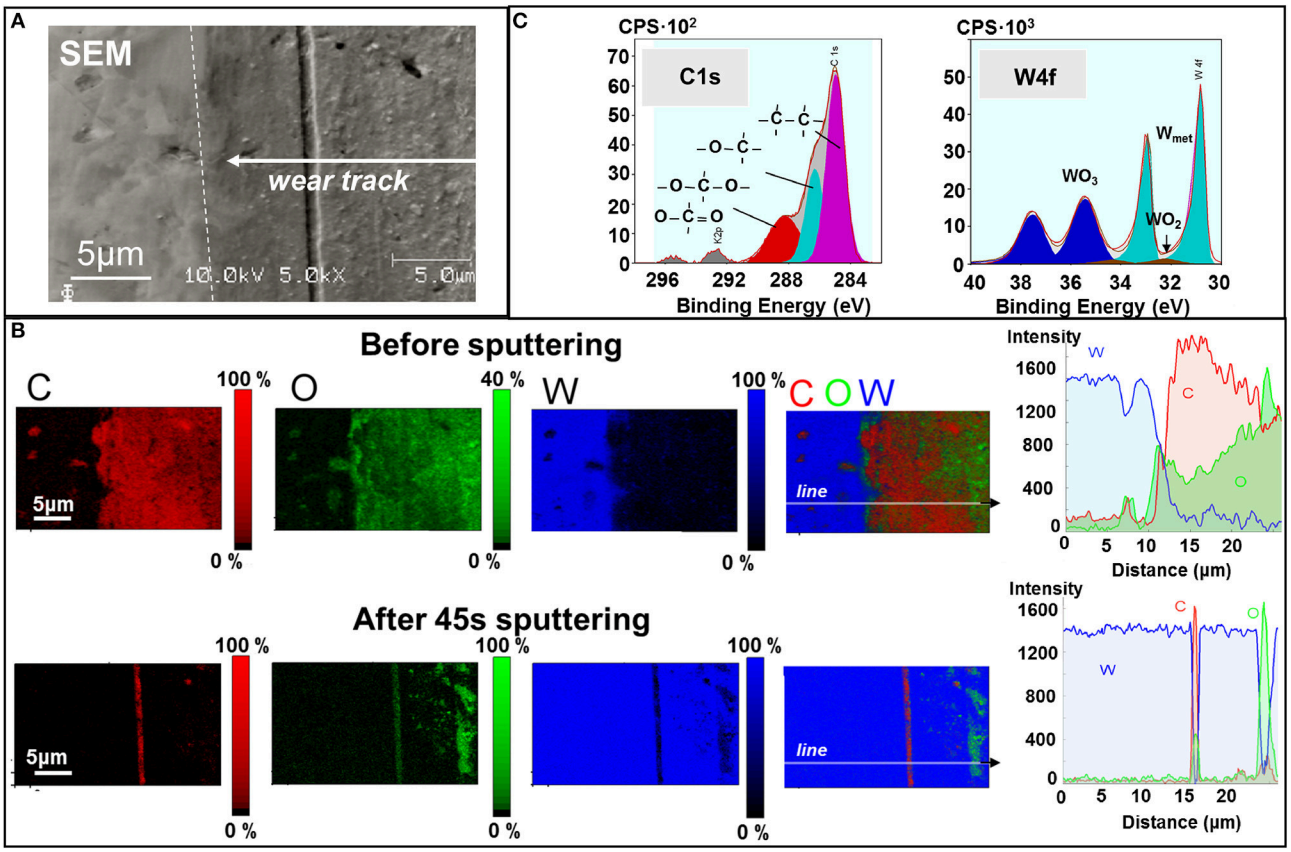

FIGURE 5 | Chemical analysis of the worn tungsten surface after hexadecane-lubricated sliding. **(A)** SEM image of the wear track on the tungsten counter surface. **(B)** Auger electron spectroscopy (AES) mapping and XPS of the wear track before and after 45 s of sputtering. **(C)** XPS detail spectra and binding states on the wear track.

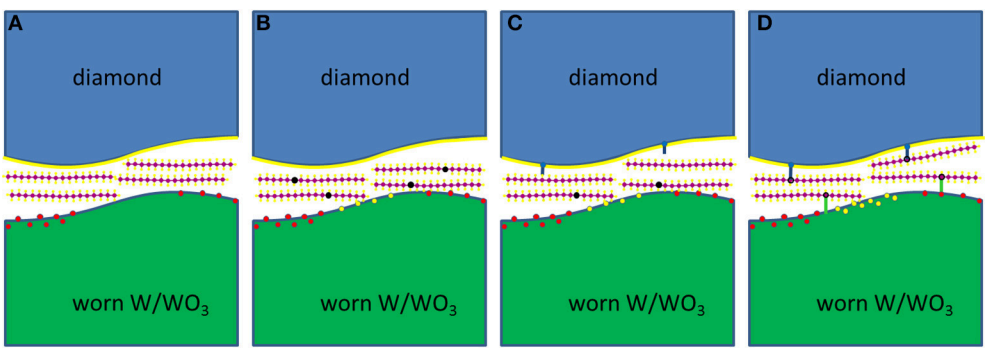

FIGURE 6 | Schematic of a probable reaction path for the radicalization and chemical adsorption of hydrocarbon molecules between W/diamond and WO_3/diamond sliding interfaces. **(A)** Sliding of diamond against the tungsten counterbody under high loads results in wear of the WO_3 material that passivates the tungsten surface. This creates reactive patches of worn W and/or WO_3. **(B)** These reactive sites can then easily radicalize the initially saturated hydrocarbon molecules. **(C)** The radicalized molecules can then remove passivating H atoms (or OH groups) from the diamond surface, resulting in the creation of reactive sites on the diamond surface. **(D)** The remaining radical molecules can then bond onto reactive sites on the diamond surface or on the worn W/WO_3 surface. The preferential bonding of the radicals on the diamond and WO_3 surfaces can eventually result in the formation of hydrocarbon layers attached to the diamond and WO_3 surfaces, while desorption of the absorbed molecules on WO_3 sites can result in the formation of molecules with O and/or OH groups, which can eventually also be adsorbed onto the diamond surface.

0.05 was recorded in the classical MD simulations. This very low friction resistance is a direct result of the hydrocarbon film, since both the absence of lubricant reactions and the formation of a WC film would result in cold welding and high friction. Quasi-static DFT calculations confirmed the classical MD results. Additional DFT calculations demonstrate that

hydrocarbon molecules can radicalize and chemisorb *via* C–O bonds on WO_3 surfaces, suggesting that the lubricant-derived hydrocarbon films also form on tungsten counter surfaces with WO_3 passivation. Our on-line tribometer experiments confirm the scenario derived from the classical and DFT simulations. In the simulation as well as in the experiment, ultralow friction of tungsten/diamond sliding contacts under $C_{16}H_{34}$ lubrication was observed. Furthermore, *ex situ* chemical analysis by means of XPS, EELS, and AES reveals evidence of the formation of a carbon-rich tribofilm on the diamond and tungsten oxide surfaces as predicted by the atomistic simulations. That no signs of the formation of WC phases were found is also in agreement with our classical MD results.

We believe that the tribochemical mechanisms reported in this article are transferable to other lubricated metal/diamond parings such as, e.g., steel/diamond combinations. There is experimental evidence in the context of *white etching crack* research that steel is also able to abstract hydrogen from mineral oils (Kuerten et al., 2016). Therefore, it is likely that the ultralow friction coefficients recorded by Mehan and Hayden (1981) for steel/diamond pairings originate from *in situ* tribochemical formation of low-friction hydrocarbon films. These films should be extremely effective under boundary lubrication conditions: while free lubricant molecules can be squeezed out of asperity contacts, chemisorbed films stay in the contact and prevent cold welding and high friction. Of course, further research for other metal/diamond combinations is now in order. The methodology and the results in this article will prove a useful guide for such future investigations.

DATA AVAILABILITY

The datasets generated for this study are available on request to the corresponding author.

AUTHOR CONTRIBUTIONS

All authors listed have made a substantial, direct and intellectual contribution to the work, and approved it for publication.

ACKNOWLEDGMENTS

We thank the Deutsche Forschungsgemeinschaft for financial support under contracts FI451, MO879, SCH425, and KO 120/12-1, as well as CRC 926 (MICOS) and DI1494. The authors would also like to thank Dr. Alfons Fischer and Dr. Alexander Brodyanski for the helpful discussions. Finally, we gratefully acknowledge the computing time granted under project-aticsi at KIT HLRII and under project No. hfr09 on the supercomputer JUROPA for some of the classical MD simulations, and under project no. hfr04 on the supercomputer JURECA for the DFT calculations at NIC Jülich Supercomputing Center.

REFERENCES

Blöchl, P. E. (1994). Projector augmented-wave method. *Phys. Rev. B* 50, 17953–17979. doi: 10.1103/PhysRevB.50.17953

Esser, J., Linde, R., and Münchow, F. (2004). Diamond-reinforced running surface for combustion rings. *MTZ Worldw.* 65, 27–28. doi: 10.1007/BF03227689

Fu, X. Y., Rigney, D. A., and Falk, M. L. (2003). Sliding and deformation of metallic glass: experiments and MD simulations. *J. Non Cryst. Solids* 317, 206–214. doi: 10.1016/S0022-3093(02)01999-3

Groot, R. D., and Warren, P. B. (1997). Dissipative particle dynamics: bridging the gap between atomistic and mesoscopic simulation. *J. Chem. Phys.* 107, 4423–4435. doi: 10.1063/1.474784

Hohenberg, P., and Kohn, W. (1964). The inhomogeneous electron gas. *Phys. Rev.* 136, B864. doi: 10.1103/PhysRev.136.B864

Juslin, N., Erhart, P., Träskelin, P., Nord, J., Henriksson, K., Salonen, E., et al. (2005). Analytical interatomic potential for modeling nonequilibrium processes in the W-C-H system. *J. Appl. Phys.* 98:123520. doi: 10.1063/1.2149492

Kennedy, M., Hoppe, S., and Esser, J. (2014). Lower friction losses with new piston ring coating. *MTZ Worldw.* 75, 24–29. doi: 10.1007/s38313-014-0135-7

Kim, Y., Park, H., An, J. U., Kan, T.-S., and Park, J. (2011). Development of nano diamond polymer coating on piston skirt for fuel efficiency. *SAE Int. J. Engines* 4, 2080–2086. doi: 10.4271/2011-01-1401

Kohn, W., and Sham, L. J. (1965). Multiple pilomatricoma with perforation. *Phys. Rev.* 140, A1133–A1138. doi: 10.1103/PhysRev.140.A1133

Korres, S., and Dienwiebel, M. (2010). Design and construction of a novel tribometer with online topography and wear measurement. *Rev. Sci. Instrum.* 81:063904. doi: 10.1063/1.3449334

Kresse, G., and Hafner, J. (1993). *Ab initio* molecular dynamics for liquid metals. *Phys. Rev. B* 47, 558–561. doi: 10.1103/PhysRevB.47.558

Kresse, G., and Hafner, J. (1994). *Ab initio* molecular-dynamics simulation of the liquid–metal–amorphous–semiconductor transition in germanium. *Phys. Rev. B* 49, 14251–14269. doi: 10.1103/PhysRevB.49.14251

Kresse, G., and Joubert, D. (1999). From ultrasoft pseudopotentials to the projector augmented-wave method. *Phys. Rev. B* 59, 1758–1775. doi: 10.1103/PhysRevB.59.1758

Kuerten, D., Winzer, N., Kailer, A., Pfeiffer, W., Spallek, R., and Scherge, M. (2016). *In-situ* detection of hydrogen evolution in a lubricated sliding pin on disk test under high vacuum. *Tribol. Int.* 93, 324–331. doi: 10.1016/j.triboint.2015.07.028

Kuwahara, T., Romero, P. A., Makowski, S., Weihnacht, V., Moras, G., and Moseler, M. (2019). Mechano-chemical decomposition of organic friction modifiers with multiple reactive centres induces superlubricity of ta-C. *Nat. Commun.* 10:151. doi: 10.1038/s41467-018-08042-8

Linsler, D., Kümmel, D., Nold, E., and Dienwiebel, M. (2017). Analysis of the running-in of thermal spray coatings by time-dependent stribeck maps. *Wear* 376–377, 1467–1474. doi: 10.1016/j.wear.2017.02.026

Mehan, R. L., and Hayden, S. C. (1981). Friction and wear of diamond materials and other ceramics against metal. *Wear* 74, 195–212. doi: 10.1016/0043-1648(81)90163-0

Pastewka, L., Moser, S., Gumbsch, P., and Moseler, M. (2011). Anisotropic mechanical amorphization drives wear in diamond. *Nat. Mater.* 10, 34–38. doi: 10.1038/nmat2902

Pastewka, L., Moser, S., Moseler, M., Blug, B., Meier, S., Hollstein, T., et al. (2008). The running-in of amorphous hydrocarbon tribocoatings: a comparison between experiment and molecular dynamics simulations. *Zeitschrift Fuer Met. Res. Adv. Tech.* 99, 1136–1143. doi: 10.3139/146.101747

Perdew, J. P., Burke, K., and Ernzerhof, M. (1996). Generalized gradient approximation made simple. *Phys. Rev. Lett.* 77, 3865–3868. doi: 10.1103/PhysRevLett.77.3865

Persson, B. N. J. (2006). Contact mechanics for randomly rough surfaces. *Surf. Sci. Rep.* 61, 201–227. doi: 10.1016/j.surfrep.2006.04.001

Rigney, D. A. (2000). Transfer, mixing and associated chemical and mechanical processes during the sliding of ductile materials. *Wear* 245, 1–9. doi: 10.1016/S0043-1648(00)00460-9

Scherge, M., Shakhvorostov, D., and Pöhlmann, K. (2003). Fundamental wear mechanism of metals. *Wear* 255, 395–400. doi: 10.1016/S0043-1648(03)00273-4

Stoyanov, P., Merz, R., Romero, P. A., Wählisch, F. C., Abad, O. T., Gralla, R., et al. et al. (2015). Surface softening in metal-ceramic sliding contacts: an experimental and numerical investigation. *ACS Nano* 9, 1478–1491. doi: 10.1021/nn505968m

Stoyanov, P., Romero, P. A., Järv, T. T., Pastewka, L., Scherge, M., Stemme, P., et al. (2013a). Experimental and numerical atomistic investigation of the third body formation process in dry tungsten/tungsten-carbide tribo couples. *Tribol. Lett.* 50, 67–80. doi: 10.1007/s11249-012-0085-7

Stoyanov, P., Stemmer, P., Järvi, T. T., Merz, R., Romero, P. A., Scherge, M., et al. (2013b). Friction and wear mechanisms of tungsten-carbon systems: a comparison of dry and lubricated conditions. *ACS Appl. Mater. Interfaces* 5, 6123–6135. doi: 10.1021/am4010094

Stoyanov, P., Stemmer, P., Järvi, T. T., Merz, R., Romero, P. A., Scherge, M., et al., et al. (2014). Nanoscale sliding friction phenomena at the interface of diamond-like carbon and tungsten. *Acta Mater.* 67, 395–408. doi: 10.1016/j.actamat.2013.12.029

Venkateswarlu, K., Rajinikanth, V., Naveen, T., Sinha, D. P., Atiquzzaman, S., and Ray, A. K. (2009). Abrasive wear behavior of thermally sprayed diamond reinforced composite coating deposited with both oxy-acetylene and HVOF techniques. *Wear* 266, 995–1002. doi: 10.1016/j.wear.2009.02.001

Wang, L., Gao, Y., Xue, Q., Liu, H., and Xu, T. (2005). Effects of nano-diamond particles on the structure and tribological property of Ni-matrix nanocomposite coatings. *Mater. Sci. Eng. A* 390, 313–318. doi: 10.1016/j.msea.2004.08.033

Yin, S., Xie, Y., Cizec, J., Ekoi, E. J., Hussain, T., Dowling, D. P., et al. (2017). Advanced diamond-reinforced metal matrix composites *via* cold spray: properties and deposition mechanism. *Compos. Part B Eng.* 113, 44–54. doi: 10.1016/j.compositesb.2017.01.009

Conflict of Interest Statement: The authors declare that the research was conducted in the absence of any commercial or financial relationships that could be construed as a potential conflict of interest.